Journal of Molecular Catalysis A: Chemical 346 (2011) 29–38

Contents lists available at ScienceDirect

Journal of Molecular Catalysis A: Chemical

journal homepage: www.elsevier.com/locate/molcata

Promotion effect of tungsten oxide on SCR of NO with NH_3 for the V_2O_5–WO_3/$Ti_{0.5}Sn_{0.5}O_2$ catalyst: Experiments combined with DFT calculations

Chuanzhi Sun [a], Lihui Dong [a], Wujiang Yu [a], Lichen Liu [a], Hao Li [a], Fei Gao [b,*], Lin Dong [a,b,**], Yi Chen [a]

[a] Key Laboratory of Mesoscopic Chemistry of Ministry of Education, School of Chemistry and Chemical Engineering, Nanjing University, Nanjing 210093, PR China
[b] Center of Modern Analysis, Nanjing University, Nanjing 210093, PR China

ARTICLE INFO

Article history:
Received 10 February 2011
Received in revised form 12 June 2011
Accepted 16 June 2011
Available online 23 June 2011

Keywords:
V_2O_5–WO_3/TS catalyst
Brønsted acid sites
In situ IR
$NO + NH_3 + O_2$
DFT

ABSTRACT

Binary metal oxides V_2O_5–WO_3 supported on $Ti_{0.5}Sn_{0.5}O_2$ (hereafter denoted as TS) catalysts have been characterized by XRD, LRS, TPR, NH_3-TPD, in situ FT-IR and the micro-reactor test for the removal of NO by NH_3. The results suggest that: (1) both vanadium oxide and tungsten oxide (loadings $\leq$0.5 mmol/100 m^2 TS) are highly dispersed on TS support. (2) The reduction temperature of vanadium species becomes higher due to the formation of the V–O–W bonds. (3) With the loading amounts of WO_3 increasing, the amounts of the Brønsted acid sites increase, while the amounts of Lewis acid sites decrease. The strength of Brønsted acid sites is little influenced by the tungsten species which is further proved by the density functional theory (DFT) calculation results. The adsorption of NO is little changed after WO_3 addition. Further increase of WO_3 (loadings $\geq$ 1.0 mmol/100 m^2 TS) results in the formation of crystalline WO_3 and they will cover the vanadium oxide species on the surface of the catalysts. (4) The activity of "$NO + NH_3 + O_2$" reaction is tightly related to the amounts of the Brønsted acid sites: the higher SCR activities should be attributed to the larger amounts of Brønsted acid sites when WO_3 are highly dispersed. When the crystalline WO_3 form, they cover the surface of the catalysts, and lead to the decrease of the activities.

1. Introduction

NO_x is an air pollutant gas to be responsible for town smog and acid rain, thus it is important to remove NO_x contained in the exhaust gases from the stationary and mobile emission sources [1]. The selective catalytic reduction (SCR) of NO_x by NH_3 is to date the best developed and wide-spread method for NO_x removal from stationary sources [2,3]. In this process, NO_x contained in the flue gases is reduced by injecting NH_3 to produce innoxious nitrogen and water.

V_2O_5 based catalysts are industrially important catalysts used for the selective reduction of NO_x. Commonly, tungsten oxide species are added to V_2O_5 based catalysts to improve the activity and N_2 selectivity for NO reduction by NH_3 in the presence of oxygen [4,5]. The results in the literature report that WO_3 behave as both "structural" and "chemical" promoters for the catalysts [3]. As the "structural" promoters, it is acknowledged that suitable amount of WO_3 can stabilize the anatase phase of TiO_2 and preserve the surface characteristic of the catalysts [6]. However, as the "chemical" promoters, several questions about the effect of WO_3 are still controversial. Amiridis et al. suggest that the addition of WO_3 can provide much more Brønsted acidic sites compared with other metal oxides, which is thought to be the reason why the activities are higher than that of other metal oxides [7]. In contrast to their studies, Ramis et al. suggest that Brønsted acidity is not a necessary requirement for SCR activity [6,8,9], and ammonia is activated for SCR by coordination over Lewis acidic sites. In addition, some other literature report that the acid strength is also one of the important factors for the SCR reaction [10–12], whereas the influence of WO_3 on the strength of the acid in the catalysts has scarcely been studied. Besides the surface acidity, the reducibility of vanadia species is also thought to be responsible for the activity of the SCR reaction. Alemany et al. point out that the ternary catalysts are more active than the corresponding binary ones because of the synergetic operation between vanadium oxide and tungsten oxide species which leads to the reduction of vanadium species at lower temperatures in the SCR reaction [13].

TiO_2 with the crystalline form of anatase suffers from lack of abrasion resistance and poor mechanical strength as a support [14]. Although the addition of WO_3 can stabilize the anatase TiO_2, it still transforms to rutile-structured TiO_2 during operation at high

* Corresponding author. Tel.: +86 25 83592290; fax: +86 25 83317761.
** Corresponding author at: Key Laboratory of Mesoscopic Chemistry of Ministry of Education, School of Chemistry and Chemical Engineering, Nanjing University, Nanjing 210093, PR China. Tel.: +86 25 83592290; fax: +86 25 83317761.
E-mail addresses: gaofei@nju.edu.cn (F. Gao), donglin@nju.edu.cn (L. Dong).

1381-1169/$ – see front matter © 2011 Elsevier B.V. All rights reserved.
doi:10.1016/j.molcata.2011.06.004

temperatures and results in deterioration [15]. Consequently, various methods were devised to directly produce rutile-structured TiO_2-containing mixed oxides, which is more stable than anatase TiO_2 and possess larger BET surface area than the rutile-structured TiO_2 does. Recently, $Ti_xSn_{1-x}O_2$ system has emerged as attractive materials for several applications, such as low-voltage varistor, gas sensor, and photocatalysis [16–18]. $Ti_xSn_{1-x}O_2$ system is found to be the rutile-structure, and this is important when one considers the use of the catalyst over a long time periods [19]. In our studies, $Ti_xSn_{1-x}O_2$ system was chosen as a support to replace TiO_2 for its thermal stability.

In the present study, a series of V_2O_5–WO_3/TS catalysts have been prepared by co-impregnation method, and vanadium–tungsten interactions are adjusted by varying the tungsten loading. The influence of tungsten addition on the surface acidity, as well as the reducibility of the catalyst, has been explored by using in situ Fourier-transform infrared spectroscopy of chemisorbed NH_3 (NH_3-adsorbed in situ FT-IR), temperature programmed desorption of NH_3 (NH_3-TPD), and hydrogen temperature-programmed reduction (H_2-TPR). The relationship between the surface properties and the catalytic activity of the catalyst is discussed. Additionally, density functional theory (DFT) calculations, which are popularly used to understand the structural aspects of the catalyst [20], the nature of the active site [21,22], and the reaction mechanism [23,24], are carried out to complement our experimental results.

2. Experimental

2.1. Sample preparation

TS support was prepared by traditional co-precipitation method. $NH_3{\cdot}H_2O$ (aq) was added to the mixed aqueous solutions of $TiCl_4$ and $SnCl_4$ under vigorous stirring. The precipitate was washed with deionized water until no Cl^- could be detected by $AgNO_3$ solution, then dried at 110 °C for 12 h and calcined at 550 °C for 4 h in flowing air. The BET surface area of the TS is about 76.6 m^2/g.

The V_2O_5–WO_3/TS catalysts were prepared by incipient-wetness impregnation on the support with the solution of NH_4VO_3 and $(NH_4)_6H_2W_{12}O_{40}$ simultaneously. The samples were vigorously stirred for 1 h and then evaporated at 80 °C until achieving a paste, which was dried at 110 °C overnight and then calcined in a muffle stove at 500 °C for 4 h in flowing air. The vanadium oxide loading was 0.5 mmol/100 m^2 TS, while tungsten oxide was 0.1, 0.5, 1.0, 2.0 mmol/100 m^2 TS. The nomenclature adopted for the catalyst was 05V*x*W/TS, where the "*x*" indicated the loading amount of tungsten oxide.

2.2. Characterization

X-ray powder diffraction (XRD) patterns were collected using a Philips X'pert Pro diffractometer with Ni-filtered CuKα1 radiation (0.15408 nm). The X-ray tube was operated at 40 kV and 40 mA.

Brunauer–Emmet–Teller (BET) surface areas were measured by nitrogen adsorption at 77 K on a Micrometrics ASAP-2020 adsorption apparatus. Before each adsorption measurement, approximate 0.1 g of a catalyst sample was degassed in a N_2/He mixture at 300 °C for 2 h.

Laser Raman spectra (LRS) were recorded by using Renishaw invia spectrometer. Raman excitation at 514.5 nm was provided by Ar^+ laser. A laser power of 20 mW at the sample was applied.

Temperature-programmed desorption of ammonia (NH_3-TPD) was carried out in a quartz U-tube reactor, detected with a thermal conductivity detector (TCD). About 0.1 g of powder catalyst was pretreated by passage of high purity helium (20 ml/min) at 500 °C for 1 h. After pretreatment, the sample was saturated with highly pure ammonia (20 ml/min) at 100 °C for 0.5 h and subsequently flushed with flowing He (20 ml/min) at 100 °C for 1.5 h to remove physical adsorbed ammonia, then the samples were heated to 600 °C in flowing He (20 °C/min).

TPR was carried out in a quartz U-tube reactor connected to a thermal conduction detector with H_2–Ar mixture (7.3% H_2 by volume) as reductant. 50 mg of sample was used for each measurement. Before switching to the H_2–Ar stream, the sample was pretreated in a N_2 stream at 100 °C for 1 h. TPR started from room temperature to 700 °C at a rate of 10 °C/min.

In situ Fourier transform infrared spectroscopy (in situ FT-IR) of NH_3 or NO adsorption was carried out on a Nicolet 5700 FT-IR instrument running at 4 cm^{-1} resolution (number of scan, 32). A thin, but intact, self-supporting wafer (≈10 mg) of the adsorbents was prepared and mounted inside a high temperature cell (HTC-3, Harrick Scientific Corporation, USA). The wafer was pretreated by N_2 (99.999%) at 400 °C for 1 h. After cooling to ambient temperature, for NH_3 adsorption, NH_3 (99.999%) was introduced into the HTC at atmospheric pressure for 30 min, then the cell was flushed by N_2 for 30 min. After that, the HTC was heated to 350 °C under N_2 atmosphere at a rate of 10 °C/min and the spectra were recorded at target temperatures. For NO adsorption, NO (>99%) was introduced into the HTC at atmospheric pressure for 30 min. After that, the HTC was heated to 350 °C at a rate of 10 °C/min and the spectra were recorded at target temperatures. The spectra were obtained by subtraction of the corresponding background reference.

2.3. Catalytic reaction

The reaction activity tests of NO selective catalytic reduction by ammonia were measured in a flow micro-reactor with a gas composition of 700 ppm NH_3, 700 ppm NO, 4% O_2 and 96% N_2 by volume at a space velocity of 180,000 ml g^{-1} h^{-1}, 100 mg catalyst was used for each measurement. The catalysts were tested from 200 °C to 350 °C and the NO concentrations before and after reaction were determined by using an N-(1-naphtyl)-ethylenediamine dihydrochloride spectrophotometer method (Saltzman method) [25].

2.4. Computational details

Onal et al. [26] report that the adsorption of small molecules, such as H_2O and NH_3, is a relatively local phenomenon and a small metal oxide cluster can sufficiently represent larger cluster surfaces. Hence, a $V_2O_9H_8$ cluster was selected as a working model of the vanadium-like surface species in the present work [27]. In this cluster, two structurally inequivalent oxygen sites, i.e., terminal vanadyl oxygen and bridging oxygen, were represented, and all of the peripheral oxygen atoms were saturated by hydrogen atoms (Fig. 1a). For the ammonia adsorption calculations, a Brønsted acidic site (V–OH) was created by adding one H atom to the V=O site of the $V_2O_9H_7$ cluster (Fig. 1b). The location of the Brønsted acidic site was selected as doubly bonded O atom since this site was considered as the most active site of the V_2O_5 cluster in the literature [21,24,28]. The calculated parameters of $V_2O_9H_8$ agree well with the crystallographic data of V_2O_5 (Table 1), accordingly, the cluster model seems to be a reasonable representation of the surface vanadium. It is known that tungsten oxide forms solid solutions with vana-

Table 1
Calculated and crystallographic structural parameters (Å) of V–O–V subunit in V_2O_5.

	DFT calculations	Crystallographic data
$d_{V=O}$	1.58	1.58
$d_{V-O\ bridge}$	1.82	1.88

Fig. 1. The optimized structure of the cluster (a) $V_2O_9H_8$; the structure of the optimized Brønsted acidic (b) $V_2O_9H_8$ cluster and (c) VWO_9H_7 cluster.

dium oxide [29]. It can be expected that, similarly as MoO_3–V_2O_5 solid solution [30,31], WO_3–V_2O_5 solid solution forms by substitution of some W atoms for V ones in the vanadium oxide structure [32] and then the VWO_9H_7 cluster (Fig. 1c) is selected to represent the V–O–W system. Therefore, it is reasonable to choose VWO_9H_7 cluster as the working model in the present work.

All calculations were carried out using the Gaussian'03 package [33]. The geometries of all stationary points were optimized with the B3LYP density functional [34–36]. Relativistic effective core potential (ECP) was employed for V and W with the standard LanL2DZ basis set, and all of the other atoms were described with 6-31G(d,p) basis set. The optimized geometries of the clusters used in the DFT calculations are shown in Fig. 1. In all of the calculations, V1, O1, V2, O3, H1, W atoms and the bridge oxygen atom (O2) were relaxed while the rest of the cluster atoms were kept fixed.

3. Results and discussion

3.1. SCR activity

Fig. 2 shows the activities of 05V*x*W/TS catalysts for the SCR reaction. As displayed in Fig. 2, the 05 W/TS catalyst shows negligible activity below 350 °C, while 05V/TS catalyst exhibits 20–40% in NO conversion in the range of 200–350 °C. Hence, regarding all the catalysts, vanadium oxide species are considered as the main active species below 350 °C. When the tungsten oxide is introduced into the 05 V/TS sample, the NO conversions change greatly depending on the tungsten loading amounts. With the loading amounts of tungsten oxides increasing, the NO conversion increases at first and decreases subsequently, indicating that increasing the WO_3 loading cannot always promote the catalytic activity and a maximum is reached at the suitable tungsten loading. Among all the 05V*x*W/TS samples, the NO conversion of 05V05W/TS is the highest. According to the literature [7–13], the activities of catalysts for the SCR reaction should be related to the surface physicochemical properties

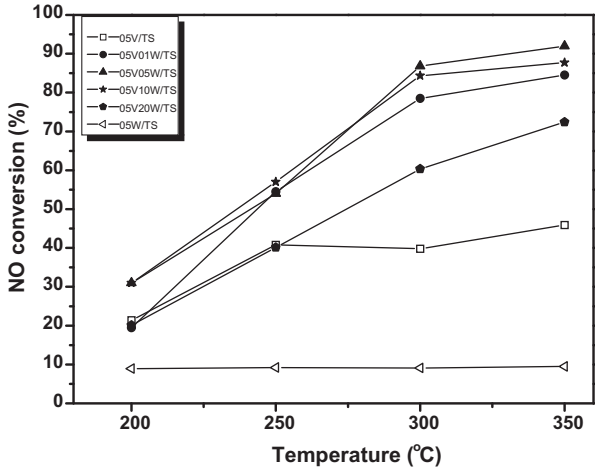

Fig. 2. Activities of the 05V/TS, 05V*x*W/TS and 05W/TS catalysts for the SCR reaction of NO + NH_3 + O_2.

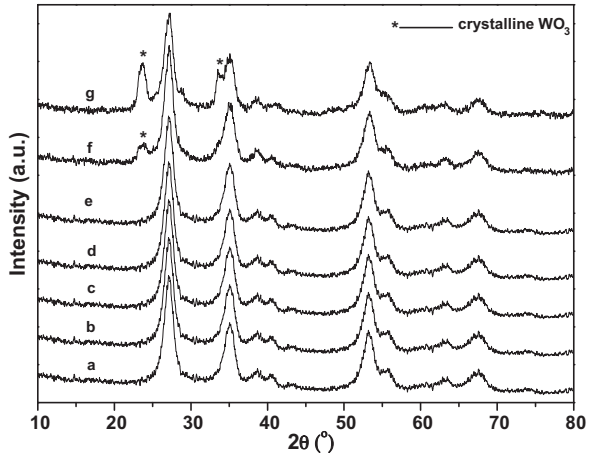

Fig. 3. The X-ray diffraction patterns of (a) TS; (b) 05W/TS; (c) 05V/TS; (d) 05V01W/TS; (e) 05V05W/TS; (f) 05V10W/TS; (g) 05V20W/TS.

of the catalysts. Along this line, the catalysts were characterized as below.

3.2. The state of surface species of the catalysts

The X-ray diffraction patterns of the samples are shown in Fig. 3. There are no typical diffraction peaks of crystalline V_2O_5 for all samples, indicating the vanadium oxide species present as a highly dispersed state on TS support. Whereas, for tungsten oxide species, the results reveal that the WO_3 exist as highly dispersed species in the 05V01W/TS and 05V05W/TS samples. When the WO_3 loading amounts are higher than 0.5 mmol/100 m^2 TS, the existence of crystalline WO_3 are obvious for the 05V10W/TS and 05V20W/TS samples and the peak intensities increase with the increasing of WO_3 loading amounts.

To further investigate the structures of the surface species, the Raman spectrum has been performed and the results are shown in Fig. 4. Two peaks at 956 cm^{-1} and 802 cm^{-1}, assigned to W=O stretching mode of the tungsten oxide species and the presence of the polymeric tungsten oxide species, respectively, can be detected in 05W/TS sample [13,37]. For 05V/TS sample, only a weak band at about 1012 cm^{-1} can be observed, which is attributed to the stretching vibrations of short V=O band [38]. When the vanadium oxide and tungsten oxide are co-supported on the support, a new peak at 913 cm^{-1} appears in all of the 05V*x*W/TS samples. Compared with 05W/TS sample, the scattering peak of tungsten oxide (WO_3) at 802 cm^{-1} disappears in 05V05W/TS sample, which implies the absence of the polymeric tungsten oxide species. This should be due to the interaction between vanadium oxide and tungsten oxide species that leads to the vanadium dispersing within the W–O–W chains of tungsten oxide species and forming V–O–W chains. Therefore, it is reasonable to suggest that the new peak at 913 cm^{-1} should be due to the formation of V–O–W bond.

With further increasing of the WO_3 loadings, it can be seen that the peak at 802 cm^{-1} appears in the spectrum of 05V10W/TS sample indicating the W–O–W bond forms on the surface of the catalysts and the peak intensity becomes more insensitive in the

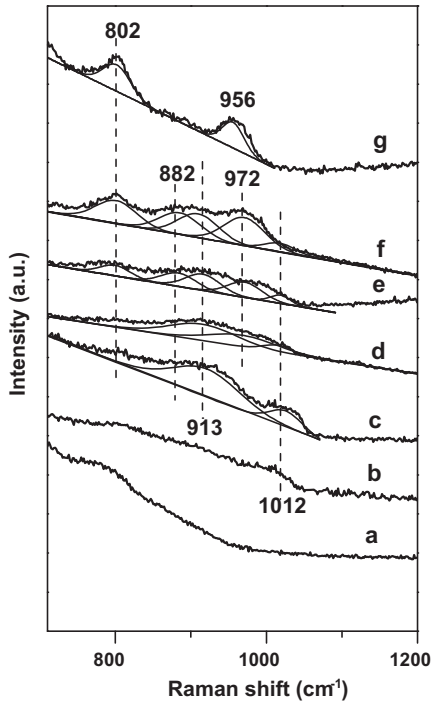

Fig. 4. The Laser Raman spectra of (a) TS (b) 05V/TS; (c) 05V01W/TS; (d) 05V05W/TS; (e) 05V10W/TS; (f) 05V20W/TS; (g) 05W/TS.

spectrum of 05V20W/TS sample. The XRD results have revealed that the crystalline WO_3 appears on the surface of the 05V10W/TS and 05V20W/TS samples. It should be responsible for the appearance of the W–O–W bond. Meanwhile, it is noteworthy that a new peak at 882 cm^{-1} occurs obviously in 05V20W/TS sample. According to the literature [39], the simultaneous appearance of the 882, 913 and 972 cm^{-1} should be attributed to the tungsten oxide species presenting on the surface of the vanadium oxide species. Hence, it can be concluded that partial surface of the 05V*x*W/TS samples would be covered gradually by the crystalline WO_3 with the tungsten oxide loadings increasing. From above results, the gradually changing states of the V_2O_5–WO_3 supported on TS could be illustrated in Fig. 5. Before the addition of WO_3 (Fig. 5a), vanadium oxides species are dispersed on the TS support. After WO_3 addition (Fig. 5b), V–O–W species form, and they increase with the loading amounts of WO_3 increasing (Fig. 5c). When the crystalline WO_3 appear, they will gradually cover the surface vanadium oxides species (Fig. 5d).

Generally, the structures of surface species should be correlated to the activities of the catalysts. Broclawik et al. have reported that the presence of W atoms in vanadia-like surface facilitated the formation of OH groups [40]. Amiridis et al. suggested that the presence of a Brønsted acid site in close proximity with the vanadium site would result in a promoting effect on SCR activity [7]. The Laser Raman spectra results suggest that when WO_3 are introduced into the catalysts, the V–O–W bond forms. Thus, it can be concluded from our results that the tungsten atoms dispersing within the V–O–V chains may produce Brønsted acid sites which are adjacent to the vanadium active sites, and make the catalysts more effective than the pure V_2O_5 based catalysts. With the WO_3 loadings further increasing, the excessive crystalline WO_3 cover the surface of the active sites, which lead to the decrease of the activities.

3.3. Reducibility of the vanadium oxide species

The activities of the catalysts are usually close to the reduction properties of the catalysts. The easier reduction of the vanadium oxide species will result in the higher activities. To investigate the effect of WO_3 on the reduction behaviors of vanadium oxide species, the H_2-TPR experiment of 05V*x*W/TS catalysts were performed and the results are shown in Fig. 6. For the pure TS support, the H_2 consumption peak at 627 °C should be attributed to the reduction of the support. For the 05V/TS catalyst, the reduction temperature of the peak (at 627 °C) remains unchanged. After the addition of WO_3, with the loading of WO_3 increasing, this peak gradually shifts to lower temperature region which should be due to the interaction between the tungsten oxide and the TS support.

At the low temperature region (100–400 °C, shown in Fig. 6B), in the profile of the pure TS support, a reduction peak at 310 °C can be observed, corresponding to the reduction of the surface Ti^{4+} and Sn^{4+}. In the profile of 05V/TS sample, a new reduction peak appears at about 273 °C, which is attributed to the reduction of vanadium oxide species. It is noteworthy that this peak gradually shifts to 294 °C with the loading of WO_3 increasing. According to the LRS results, the increase of the reduction temperature of vanadium oxide species may due to the formation of the V–O–W bonds. To further investigate the surface states of the vanadium oxide and tungsten oxide species, the H_2 consumption peak areas are calculated and listed in Table 2. It can be seen that the peak areas first remain unchanged when the loading of WO_3 is below 0.5 mmol/100 m^2 TS, and then the peak areas decrease gradually

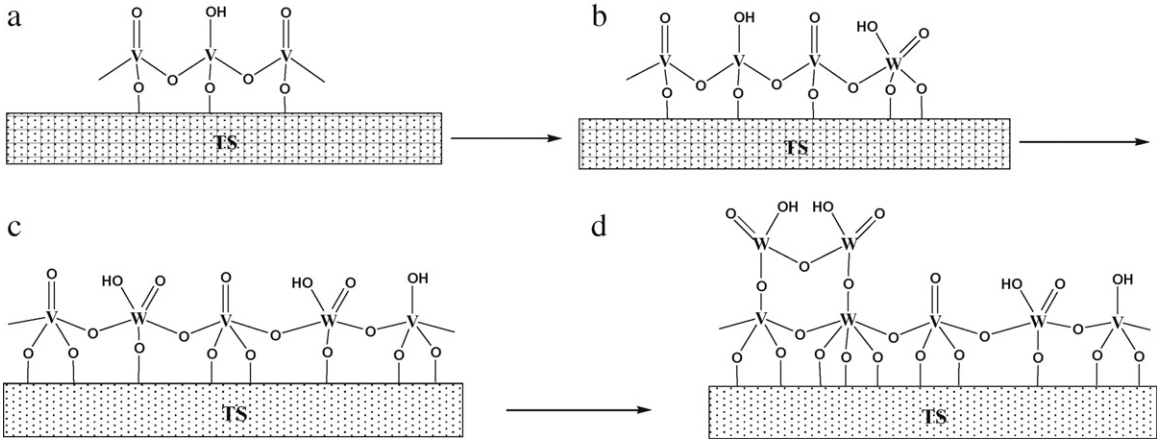

Fig. 5. The gradually changing states of the V_2O_5–WO_3 supported on TS with increasing the loading amounts of WO_3.

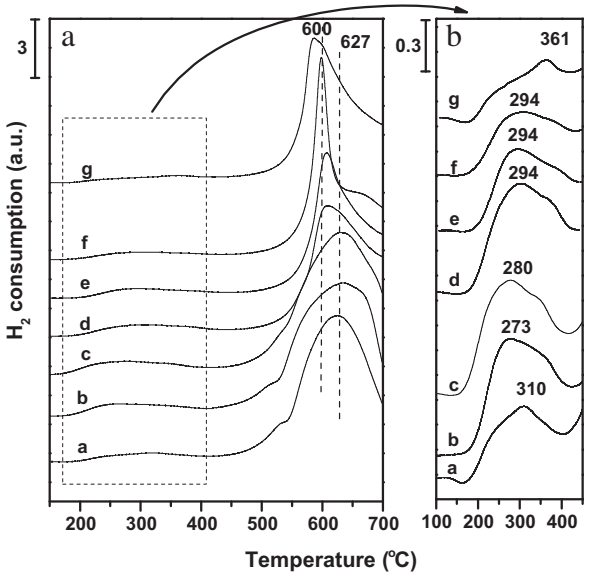

Fig. 6. The H_2-TPR profiles of (a) TS; (b) 05V/TS; (c) 05V01W/TS; (d) 05V05W/TS; (e) 05V10W/TS; (f) 05V20W/TS; (g) 05W/TS.

with the loading amounts of WO_3 increasing. Combined with the LRS results, it can be elucidated that the decrease of the peak areas should be associated with the formation of crystalline WO_3 which cover the surface of the catalyst, and prevent the reduction of vanadium oxide species. From TPR results, it can be concluded that the addition of WO_3 cannot facilitate the reduction of the vanadium oxide species. Consequently, the reduction properties should not be responsible for the higher activities of the V_2O_5–WO_3/TS catalysts in the SCR reaction.

3.4. NO adsorption on the surface of the catalysts

The in situ FT-IR information about adsorption of NO is given in Fig. 7. The peaks of N=O (ca. 1630 cm^{-1} and 1600 cm^{-1}) for bridging bidentate nitrate, $NO_{2,as}$ (ca. 1294 cm^{-1} and 1273 cm^{-1}) for bridging bidentate and/or chelating bidentate nitrate, split υ_3 mode (ca. 1220 cm^{-1}) for bridging bidentate and/or chelating bidentate nitrate and $N_2O_2^{2-}$ (ca. 1745 cm^{-1} and 1256 cm^{-1}) can be observed at low temperatures [41,42]. Furthermore, at low temperatures, the obvious difference between the spectra of 05V/TS and 05V*x*W/TS samples is that the peak at ca. 1294 cm^{-1} corresponding to the $NO_{2,as}$ vibration becomes stronger after the WO_3 addition. However, with the temperature increasing, many nitrate species desorbed or decompose easily including the peak at 1294 cm^{-1}. When the temperature is above 250 °C, for 05V/TS and 05V*x*W/TS samples, all the FT-IR spectra are similar, only the peaks at about 1630 cm^{-1} and 1600 cm^{-1} can be observed. These results indicate that the influence of WO_3 addition on the adsorbed nitrate species may be negligible at the reaction temperature. In the literature [4,43–45], it is also reported that adsorption of NO is negligible at the reaction temperature in the presence of NH_3, and NH_3 adsorbing on Brønsted acid sites is the important step for SCR reaction. Thus, we mainly focus on studying the factors which influence the adsorption of NH_3 on the catalysts in the following text.

3.5. Surface acidity

3.5.1. Amounts of the surface acid sites

To investigate the influences of tungsten species on the surface acidic properties, NH_3-IR spectra of 05V/TS and 05V*x*W/TS samples were conducted (as shown in Fig. 8). It can be seen that there are two absorption peaks in the profiles of the catalysts. Among them, the peaks at 1410–1456 cm^{-1} region are assigned to N–H bending vibration of NH_3 chemisorbed on Brønsted acid sites [46], while the peaks at 1220–1240 cm^{-1} region are assigned to N–H vibration of NH_3 chemisorbed on Lewis acid sites [47]. The areas of the two kinds of peak and the ratio of the Brønsted acid sites to the Lewis acid sites are shown in Table 3. As can be seen, in the 05V/TS and 05W/TS samples, the ratio is ~3.4. In the 05V01W/TS and 05V05W/TS samples, the ratio is ~7.3, and this value becomes a little larger with the tungsten species increasing. From the results, it can be concluded that the amounts of Brønsted acid sites have increased after the tungsten oxide addition, and a few addition of tungsten species results in a sharp increase of the Brønsted acid sites. Similar to this phenomenon, Amiridis et al. also report that the amounts of the Brønsted acid sites of V_2O_5–WO_3/TiO_2 catalyst are more than the combined amounts of the WO_3/TiO_2 and V_2O_5/TiO_2 samples [7]. Thus, some new Brønsted acid sites may be generated due to the V_2O_5–WO_3 interaction. Recalling our LRS results, the generation of new Brønsted acid sites may be due to the formation of the V–O–W bond. This is also a good agreement with the DFT calculation results reported by Broclawik et al. [40].

Fig. 9 presents the NH_3-TPD profiles of 05V*x*W/TS samples with different loadings of tungsten oxides. Two broad peaks at 180 °C and 465 °C can be observed when the loading of WO_3 is below 0.5 mmol/100 m^2 TS, indicating that the surface of the samples contain two kinds of acid sites, i.e., weak acid sites and strong acid sites. With the increase of WO_3 loadings, the peak intensity of the weak acid sites increases. However, the peak intensity of the strong acid site firstly little changed when the loading amounts of WO_3 is below 0.5 mmol/100 m^2 TS, further increase of WO_3 results in a sudden decrease of the strong acid sites. Moreover, it can be observed that the profiles of 05V10W/TS and 05V20W/TS samples are similar to the 05W/TS sample. According to the XRD and LRS results, the reason for the sudden decrease of the strong acid sites should be attributed to the excessive WO_3 covering the surface of the catalysts.

Although the NH_3 desorption-temperature on the Brønsted acid is usually lower than that on the Lewis acid sites, NH_3-TPD still cannot distinguish the Brønsted acid sites and Lewis acid sites, i.e., the weak acid sites may contain some Lewis acid sites and the strong acid sites may contain a few Brønsted acid sites. Thus, in order to further investigate the influence of WO_3 on the amounts of the Brønsted acid sites and Lewis acid sites, the NH_3-IR and quantitative analysis of NH_3-TPD were combined to solve this prob-

Table 2
The peak areas of TS, 05V/TS, 05W/TS and 05V*x*W/TS of H_2-TPR profiles in Fig. 6B.

Sample	Peak areas
TS	38.23
05V/TS	74.77
05V01W/TS	76.39
05V05W/TS	75.5
05V10W/TS	51.82
05V20W/TS	38.44
05W/TS	21.8

Table 3
The NH_3-IR and NH_3-TPD peak areas of 05V/TS, 05W/TS and 05VxW/TS catalysts.

Sample	Lewis acid (NH_3-IR)	Brønsted acid (NH_3-IR)	B/L	Total acid (NH_3-TPD)
05V/TS	160.42	544.27	3.39	950.26
05W/TS	134.58	464.13	3.45	1174.75
05V01W/TS	104.46	755.17	7.23	1247.47
05V05W/TS	101.76	759.70	7.47	1437.18
05V10W/TS	84.48	761.31	9.01	1440.71
05V20W/TS	83.42	760.53	9.12	1438.88

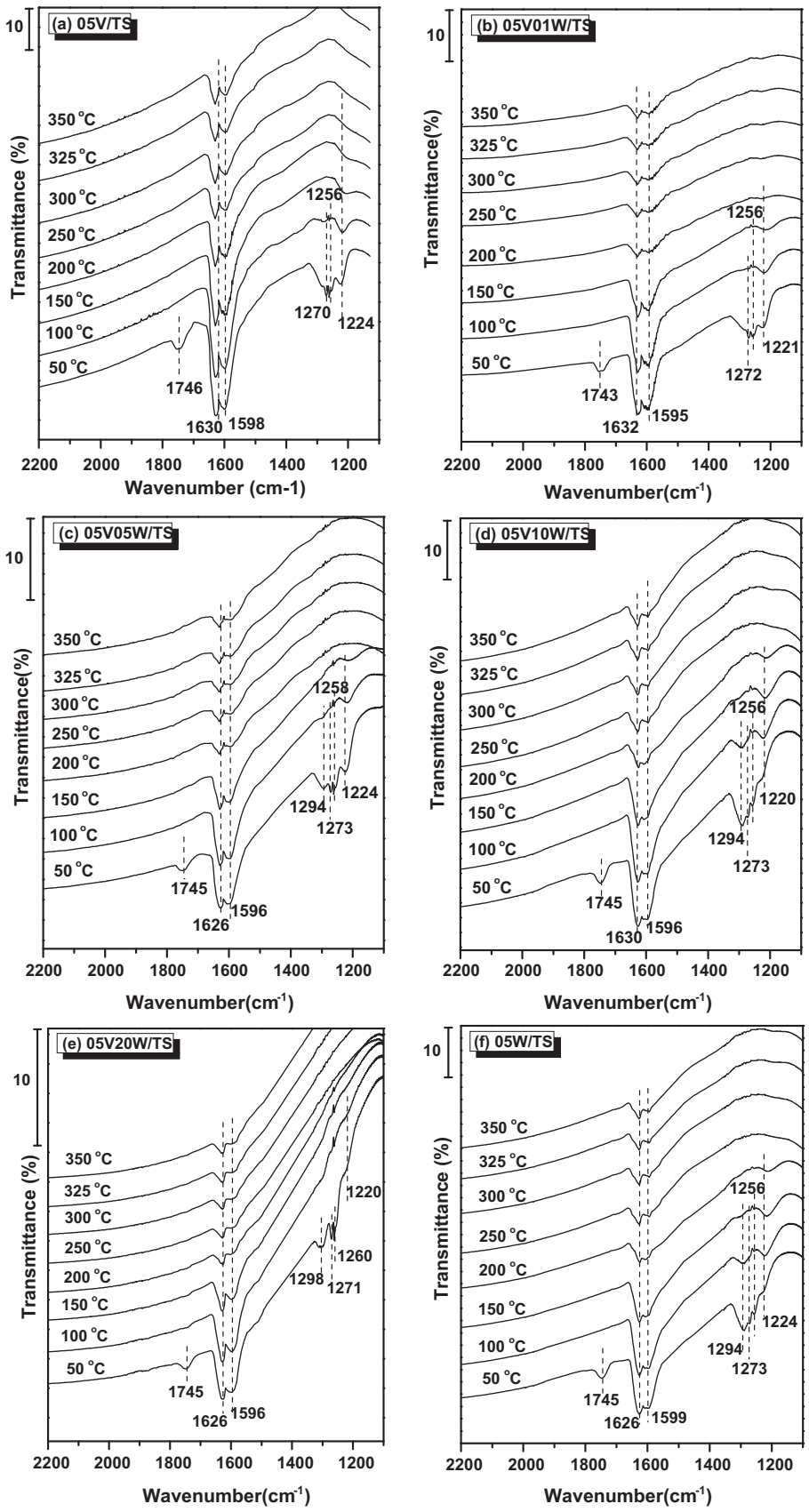

Fig. 7. The in situ FT-IR spectra of NO adsorbed on the (a) 05V/TS; (b) 05V01W/TS; (c) 05V05W/TS; (d) 05V10W/TS; (e) 05V20W/TS; (f) 05W/TS catalysts.

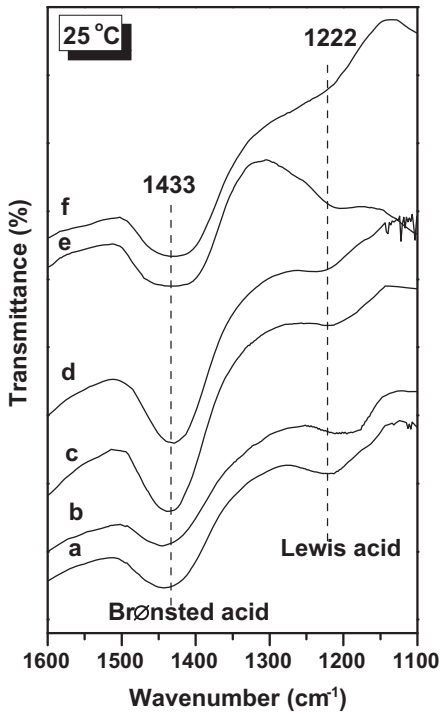

Fig. 8. NH_3-IR spectra of (a) 05V/TS; (b) 05W/TS; (c) 05V01W/TS; (d) 05V05W/TS; (e) 05V10W/TS; (f) 05V20W/TS.

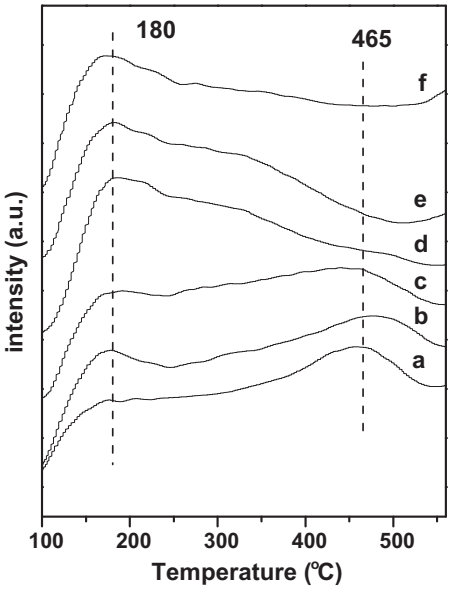

Fig. 9. NH_3-TPD profiles of (a) 05V/TS; (b) 05V01W/TS; (c) 05V05W/TS; (d) 05V10W/TS; (e) 05V20W/TS; (f) 05W/TS.

lem. It can be seen from the NH_3-TPD results (shown in Table 3) that the total amount of acid sites first increase with the loading amounts of WO_3 increasing, and then it remains almost unchanged when the loading of WO_3 is above 0.5 mmol/100 m^2 TS. Unfortunately, because the molar extinction coefficients of the Brønsted acid and Lewis acid are different, it is difficult to confirm the absolute amounts of the Brønsted and Lewis acid sites via the ratios listed in Table 3. Thus, only the relative amounts of the acid sites in each sample were calculated according to the ratios of Brønsted acid sites and Lewis acid sites. The curves representing the relative acid amounts as a function of the WO_3 loadings are shown in

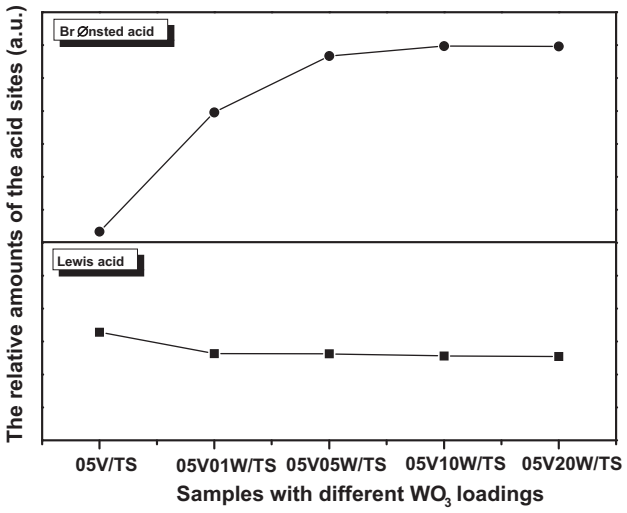

Fig. 10. The relative amounts of acid sites as a function of the WO_3 loadings.

Fig. 10. It can be seen that the amounts of Brønsted acid sites increase with WO_3 loadings increasing when the loadings of WO_3 are below 0.5 mmol/100 m^2 TS. According to the literature [7] and our experimental activity results, the increase of the Brønsted acid amounts should be responsible for the increase of the SCR activities. However, it is noteworthy that when the loadings of WO_3 are above 0.5 mmol/100 m^2 TS, although the amounts of Brønsted acid sites are increasing, the activities decrease. Combined with the LRS and XRD results, the decrease of the activities can be elucidated as following: (1) when the WO_3 exist as dispersed states, the tungsten atoms which is adjacent to the vanadium atoms will participate in the forming of V–O–W bond and increase the Brønsted acid sites amounts which lead to the increase of the activities. (2) When crystalline WO_3 form, the increases of the Brønsted acid sites are only originated from the tungsten oxides, which cannot be utilized as the active sites for the SCR reaction. Furthermore, they cover part of the vanadium atoms. Thus, the activities decrease. For the Lewis acid sites, it can be seen that its amounts decrease with the WO_3 loading increasing. Therefore, the Lewis acid sites should not be responsible for the enhancement of SCR reaction activity.

3.5.2. Strength of the surface acid sites

3.5.2.1. Experimental results. According to the kinetic mechanism proposed by Topsøe et al. [44,45], the SCR mechanism consists of two catalytic cycles. The first important step is chemisorption of NH_3 on the Brønsted acid site V–OH, and the acid strength is one of the important factors which influence the NH_3 adsorption. Thus, in situ FT-IR was conducted within a broad temperature window from 50 °C to 350 °C to investigate acid strength of the V_2O_5–WO_3/TS catalysts, as shown in Fig. 11. As can be seen, the peaks at 1423–1437 cm^{-1} region are attributed to N–H bending vibration of NH_3 chemisorbed on Brønsted acid sites [46], while the peaks at 1222–1227 cm^{-1} region are assigned to N–H vibration of NH_3 chemisorbed on Lewis acid sites [47]. For all samples, the desorption temperature of NH_3 adsorbed on the Lewis acid sites is higher than 350 °C. According to the results obtained by Lisi et al. [48], the strong acid sites adsorbing ammonia at $T > 350$ °C are not involved in the SCR reaction occurring at lower temperatures, and our results in above section also indicate that the Lewis acid sites are not the active sites for the SCR reaction of the V_2O_5–WO_3/TS catalysts. Thus, in this section the influence of WO_3 on the strength of the Brønsted acid sites is mainly investigated.

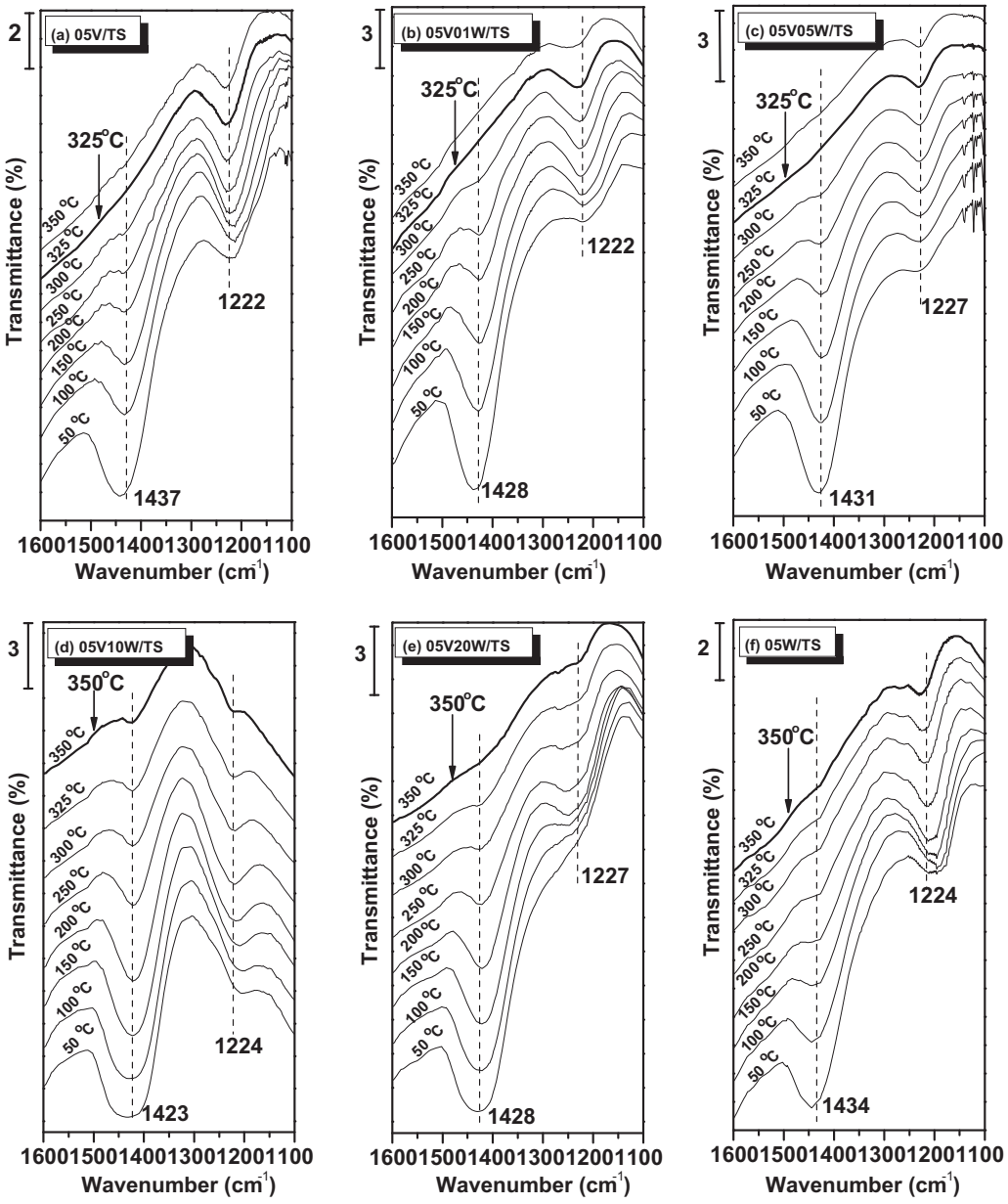

Fig. 11. The in situ FT-IR spectra of NH_3 adsorbed on the Brønsted acid sites and Lewis acid sites of (a) 05V/TS; (b) 05V01W/TS; (c) 05V05W/TS; (d) 05V10W/TS; (e) 05V20W/TS; (f) 05W/TS catalysts.

It can be seen that the increase of the temperature leads to desorption of ammonia adsorbed on Brønsted acid sites, and it is acknowledged that the different desorption temperature relates to the different strength of surface acid. Therefore, the stronger Brønsted acid strength should be related to the higher desorption temperature. According to Fig. 11 (the line which is bold represents the desorption temperature of NH_3), the order of desorption temperature of NH_3 is:

$$05V/TS = 05V01W/TS = 05V05W/TS < 05V10W/TS = 05V20W/TS = 05W/TS$$

It means that the strength of surface Brønsted acid should obey the same order. For the 05V01W/TS and 05V05W/TS samples, the desorption temperature is 325 °C which is equal to that of the 05V/TS sample. With the WO_3 loadings increasing, in the 05V10W/TS and 05V20W/TS samples, the desorption temperature is higher than 350 °C, and this temperature is similar to that of the 05W/TS sample. Taking into account the XRD and LRS results, it can be documented that the Brønsted acid strength is almost identical when WO_3 are highly dispersed on the surface of the catalyst. With the loading amounts of WO_3 increasing, the crystalline WO_3 forms and it covers the surface of the catalysts which should be the reason why the acid strength of catalysts is similar to that of the 05W/TS sample.

3.5.2.2. DFT calculation results. In this section, in order to further confirm the influence of WO_3 on the acid strength of Brønsted acid sites, the DFT calculations were carried out to prove whether the strength of Brønsted acid sites was changed under the condition of the WO_3 existence.

The acid strength of Brønsted acid sites can be estimated by the adsorption energy (E_{NH_3ad}) of NH_3 [10]. The following general computational procedures were followed: initially, both the cluster and the adsorbing molecules were fully optimized geomet-

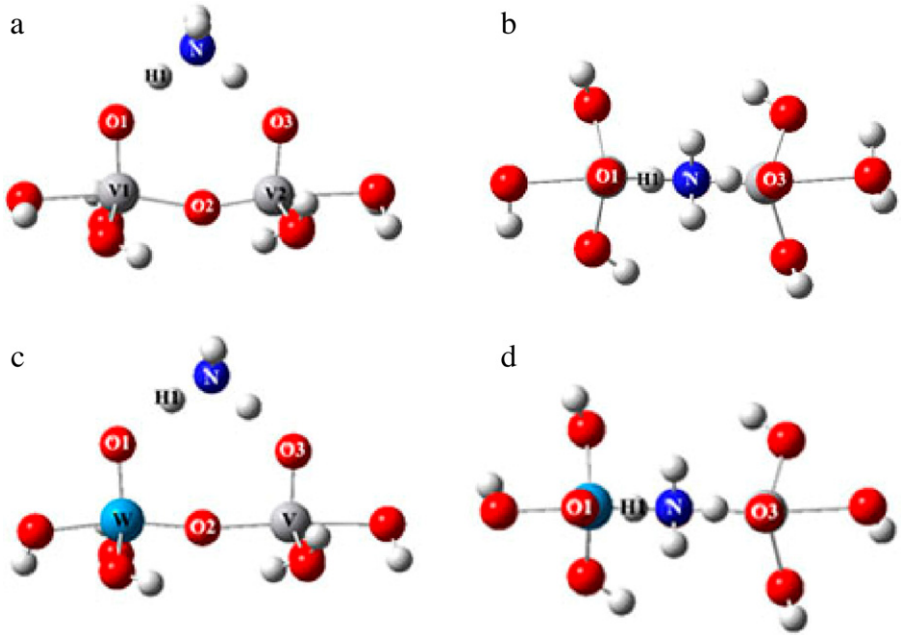

Fig. 12. Equilibrium geometry of Brønsted acidic NH_3 adsorption on $V_2O_9H_8$ cluster (a) side view; (b) top view; and on VWO_9H_7 cluster (c) side view; (d) top view.

Table 4
Comparisons of the calculated vibration frequency (cm^{-1}) data of NH_3 adsorbing on the Brønsted acid sites with experimental results.

Model	f_{NH_3} (frequency) (cm^{-1})		
	DFT calculations		Experiments
$V_2O_9H_8$	1503 (unscaled)	1444 (scaled by 0.9613[a])	1416–1441
VWO_9H_7	1509 (unscaled)	1450 (scaled by 0.9613[a])	

[a] The factor 0.9613 is cited from the book "exploring chemistry with electronic structure methods".

rically by means of the equilibrium geometry calculations. Then, the adsorbed molecules located over the active site of the cluster were fully optimized to obtain the single point energy of the system. The DFT calculation results of the vibration frequency of NH_3 adsorbed on the cluster are in good agreements with our FT-IR results as shown in Table 4, which imply that they should be reasonable models to represent the surface of the catalysts.

E_{NH_3ad} is defined as:

$$E_{NH_3ad} = E_{NH_3\text{-cluster}} - (E_{cluster} + E_{NH_3})$$

where $E_{NH_3\text{-cluster}}$, $E_{cluster}$ and E_{NH_3} are the calculated energies of $V_2O_9H_8$ (VWO_9H_7) model, NH_3 and NH_3-adsorbed $V_2O_9H_8$ (VWO_9H_7) model, respectively.

The calculated results of the $|E_{NH_3ad}|$ energy in Fig. 12a and c is 15.85 kcal mol^{-1} and 17.12 kcal mol^{-1}, respectively, and the difference of the value is only 1.27 kcal mol^{-1} which can be thought within the uncertainty of the DFT calculations. The $|E_{NH_3ad}|$ energy represents the Brønsted acid strength of the catalyst. Therefore, it can be concluded from the calculation results that Brønsted acid sites should be little changed through the synergetic operates between vanadium and tungsten oxide species.

DFT calculations combined with in situ FT-IR spectra results indicate that the acid strength of Brønsted acid sites should be little affected by the WO_3 addition. Apparently, the promotion effect of WO_3 cannot be correlated to changing the surface acid strength of the catalyst.

4. Conclusion

Based on the above results and discussion, the following main conclusions can be obtained. Brønsted acid sites should be the main active sites for SCR reaction of the V_2O_5–WO_3/TS catalysts and Lewis acid sites give little contribution to the enhancement of SCR reaction activities. The number of the Brønsted acid sites increase with the loading amounts of WO_3, and the larger amounts of Brønsted acid sites should be responsible for the higher SCR activities when WO_3 is highly dispersed. With the loading amounts of WO_3 increasing, the excessive WO_3 will cover the surface of the catalysts, consequently, the number of the surface vanadium species reduce and lead to the decrease of the activities. The acid strength of Brønsted acidic sites and the NO adsorption are little changed after WO_3 addition. The reduction temperatures of vanadium species become higher. Thus, they should not be responsible for the higher SCR activity of the V_2O_5–WO_3/TS catalysts.

Acknowledgements

The financial supports of the National Natural Science Foundation of China (Nos. 20873060, 20973091) and Jiang Su Innovative Talent Project (No. BK2008001) are gratefully acknowledged.

References

[1] V. Pârvulescu, P. Grange, B. Delmon, Catal. Today 46 (1998) 233–316.
[2] G. Busca, M.A. Larrubia, L. Arrighi, G. Ramis, Catal. Today 107–108 (2005) 139–148.
[3] L. Lietti, I. Nova, P. Forzatti, Top. Catal. 11/12 (2000) 111–122.
[4] G. Busca, L. Lietti, G. Ramis, F. Berti, Appl. Catal. B: Environ. 18 (1998) 1–36.
[5] M. Kobayashi, M. Hagi, Appl. Catal. B: Environ. 63 (2006) 104–113.
[6] S. Djerad, L. Tifouti, M. Crocoll, W. Weisweiler, J. Mol. Catal. A: Chem. 208 (2004) 257–265.
[7] M.D. Amiridis, R.V. Duevel, I.E. Wachs, Appl. Catal. B: Environ. 20 (1999) 111–122.
[8] G. Ramis, L. Yi, G. Busca, M. Turco, E. Kotur, R.J. Willey, J. Catal. 157 (1995) 523–535.
[9] G. Ramis, L. Yi, G. Busca, Catal. Today 28 (1996) 373–380.
[10] S. Yamazoe, Y. Masutani, K. Teramura, Y. Hitomi, T. Shishido, T. Tanaka, Appl. Catal. B: Environ. 83 (2008) 123–130.
[11] D.F. Jin, B. Zhu, Z.Y. Hou, J.H. Fei, H. Lou, X.M. Zheng, Fuel 86 (2007) 2707–2713.

[12] D.F. Jin, J. Gao, Z.Y. Hou, Y. Guo, X.Y. Lu, Y.H. Zhu, X.M. Zheng, Appl. Catal. A: Gen. 352 (2009) 259–264.
[13] L.J. Alemany, L. Lietti, N. Ferlazzo, P. Forzatti, J. Catal. 155 (1995) 117–130.
[14] B.M. Reddy, A. Khan, Catal. Rev. 47 (2005) 257–296.
[15] S. Djerad, M. Crocoll, S. Kureti, L. Tifouti, W. Weisweiler, Catal. Today 113 (1999) 208–214.
[16] P.R. Bueno, M.R. Cassia-Santos, L.G.P. Simões, J.W. Gomes, E. Longo, J. Am. Ceram. Soc. 85 (2002) 282–284.
[17] K. Zakrewska, Thin Solid Films 391 (2001) 229–238.
[18] F. Fresno, J.M. Coronado, D. Tudela, J. Soria, Appl. Catal. B: Environ. 55 (2005) 159–167.
[19] Z. Zhang, H. Geng, L. Zheng, B. Du, Appl. Catal. A: Gen. 284 (2005) 231–237.
[20] H.Y. Li, H.F. Wang, X.Q. Gong, Y.L. Guo, Y. Guo, G.Z. Lu, P. Hu, Phys. Rev. B 79 (2009) 193401 (1–4).
[21] F. Gilardoni, J. Weber, A. Baiker, Inter. J. Quan. Chem. 61 (1997) 683–688.
[22] I. Czekaj, O. Kröcher, G. Piazzesi, J. Mol. Catal. A: Chem. 280 (2008) 68–80.
[23] M. Anstrom, N.Y. Topsøe, J.A. Dumesic, J. Catal. 213 (2003) 115–125.
[24] M. Anstrom, J.A. Dumesic, N.Y. Topsøe, Catal. Lett. 78 (1–4) (2002) 281–289.
[25] F.S. Tang, B.L. Xu, H.H. Shi, J.H. Qiu, Y.N. Fan, Appl. Catal. B: Environ. 94 (2010) 71–76.
[26] I. Onal, S. Soyer, S. Senkan, Surf. Sci. 600 (2006) 2457–2469.
[27] A. Góra, E. Broclawik, M. Najbar, Comput. Chem. 24 (2000) 405–410.
[28] K. Hermann, M. Witko, R. Druzinic, Faraday Discuss. 114 (1999) 53–66.
[29] M. Najbar, F. Mizukami, Catal. Today 90 (2004) 93–102.
[30] A. Bielanski, M. Najbar, Appl. Catal. A: Gen. 157 (1997) 223–261.
[31] M. Najbar, J. Camra, Solid State Ionics 101–103 (1997) 707–711.
[32] M. Najbar, E. Brocławik, A. Gora, J. Camra, A. Białas, A.W. Birczynska, Chem. Phys. Lett. 325 (2000) 330–339.
[33] M.J. Frisch, G.W. Trucks, H.B. Schlegel, G.E. Scuseria, M.A. Robb, J.R. Cheeseman, J..A. Montgomery Jr., T. Vreven, K.N. Kudin, J.C. Burant, J.M. Millam, S.S. Iyengar, J. Tomasi, V. Barone, B. Mennucci, M. Cossi, G. Scalmani, N. Rega, G.A. Petersson, H. Nakatsuji, M. Hada, M. Ehara, K. Toyota, R. Fukuda, J. Hasegawa, M. Ishida, T. Nakajima, Y. Honda, O. Kitao, H. Nakai, M. Klene, X. Li, J.E. Knox, H.P. Hratchian, J.B. Cross, V. Bakken, C. Adamo, J. Jaramillo, R. Gomperts, R.E. Stratmann, O. Yazyev, A.J. Austin, R. Cammi, C. Pomelli, J.W. Ochterski, P.Y. Ayala, K. Morokuma, G.A. Voth, P. Salvador, J.J. Dannenberg, V.G. Zakrzewski, S. Dapprich, A.D. Daniels, M.C. Strain, O. Farkas, D.K. Malick, A.D. Rabuck, K. Raghavachari, J.B. Foresman, J.V. Ortiz, Q. Cui, A.G. Baboul, S. Clifford, J. Cioslowski, B.B. Stefanov, G. Liu, A. Liashenko, P. Piskorz, I. Komaromi, R.L. Martin, D.J. Fox, T. Keith, M.A. Al-Laham, C.Y. Peng, A. Nanayakkara, M. Challacombe, P.M.W. Gill, B. Johnson, W. Chen, M.W. Wong, C. Gonzalez, J.A. Pople, Gaussian 03, Revision B. 04, Gaussian, Inc., Wallingford, CT, 2004.
[34] A.D. Becke, Phys. Rev. B 38 (1988) 3098–3100.
[35] A.D. Becke, M.R. Roussel, Phys. Rev. A 39 (1989) 3761–3767.
[36] C. Lee, W. Yang, R.G. Parr, Phys. Rev. B 37 (1988) 785–789.
[37] L. Dong, Y.H. Hu, F. Xu, D. Lu, B. Xu, Z. Hu, Y. Chen, J. Phys. Chem. B 104 (2000) 78–85.
[38] G.T. Went, S.T. Oyama, A.T. Bell, J. Phys. Chem. 94 (1990) 4240–4246.
[39] J. Banaś, V. Tomašić, A.W. Birczyńska, M. Najbar, Catal. Today 119 (2007) 199–203.
[40] E. Broclawik, A. Góra, M. Najbar, J. Mol. Catal. A: Chem. 166 (2001) 31–38.
[41] Y. Chi, S.S.C. Chuang, J. Phys. Chem. B 104 (2000) 4673–4683.
[42] M. Kantcheva, J. Catal. 204 (2001) 479–494.
[43] N.Y. Topsøe, Science 265 (1994) 1217–1219.
[44] N.Y. Topsøe, H. Topsøe, J.A. Dumesic, J. Catal. 151 (1995) 226–240.
[45] N.Y. Topsøe, H. Topsøe, J.A. Dumesic, J. Catal. 151 (1995) 241–252.
[46] L.G. Pinaeva, A.P. Suknev, A.A. Budnera, E.A. Paukshitis, B.S. Balzhinimaev, J. Mol. Catal. A: Chem. 112 (1996) 115–124.
[47] G. Ramis, G. Busca, F. Bregani, P. Forzatti, Appl. Catal. 64 (1990) 259–278.
[48] L. Lisi, G. Lasorella, S. Malloggi, G. Russo, Appl. Catal. B: Environ. 50 (2004) 251–258.